Article:
He, J, Miao, J, Bai, L orcid.org/0000-0001-9016-1569 et al. (3 more authors) (2017) Effect of non-condensable gas on the startup of a loop heat pipe. Applied Thermal Engineering, 111. pp. 1507-1516. ISSN 1359-4311

https://doi.org/10.1016/j.applthermaleng.2016.07.154

Effect of non-condensable gas on the startup of a loop heat pipe

Jiang He[a], Jianyin Miao[a], Lizhan Bai[b,c], Guiping Lin[b], Hongxing Zhang[a], Dongsheng Wen[c]

[a]Beijing Key Laboratory of Space Thermal Control Technology, Beijing Institute of Spacecraft System Engineering, Beijing 100094, PR China

[b]Laboratory of Fundamental Science on Ergonomics and Environmental Control, School of Aeronautic Science and Engineering, Beihang University, Beijing 100191, PR China

[c]School of Chemical and Process Engineering, University of Leeds, Leeds, LS2 9JT, UK

Abstract: It is essential to tackle the startup issues prior to the broad application of loop heat pipes (LHPs) in both space and terrestrial surroundings. As non-condensable gas (NCG) is an important factor affecting the startup behavior, its effects on the startup performance of an ammonia-stainless steel LHP with and without preconditioning were experimentally investigated in this work. The temperature overshoot, liquid superheat and startup time were employed as the evaluation criteria. Nitrogen was selected to simulate the NCG, which was injected into the LHP at controllable amounts. Experimental results showed that with NCG presence in the LHP, the startup could only proceed in situation 1 with preconditioning, while it could proceed in situations 1, 3 or 4 without preconditioning. For the startup in situation 1, a larger NCG inventory led to much degraded startup performance, and a higher startup heat load could benefit the startup. For the startup in situation 3, i.e. the most difficult startup situation, NCG resulted in a very high temperature overshoot during the startup, which may even exceed the maximum allowable temperature to cause a startup failure. For the startup in situation 4, the existence of NCG in the vapor grooves could facilitate the evaporation of liquid there followed by a resultant very desirable startup.

Keywords: loop heat pipe; startup; experiment; non-condensable gas; thermal control

1 Introduction

As a highly efficient two-phase heat transfer device, a loop heat pipe (LHP) operates on a closed evaporation-condensation cycle and utilizes the capillary force developed in a fine porous wick to realize the circulation of the working fluid [1, 2]. Compared with conventional heat pipes, it possesses a variety of advantages such as high heat transfer capacity, long distance heat transport, and flexible thermal link, as well as strong anti-gravity capability. It has been traditionally adopted to tackle the thermal management problems of spacecraft, and successfully applied in many space missions [3-7]. However, a few unfavorable phenomena including abnormal operating temperature rise, difficult startup and operation failure were observed in several LHPs during on-orbit or ground operations [8-12]. The reliability and lifespan issues have become the major challenges for their wide space applications, especially in the next generation long life spacecraft whose design life is 15 years or even longer.

Learning from over half a century's experience on conventional heat pipes [13-16], the presence of non-condensable gas (NCG) is considered as one of the main causes for the performance degradation and reduced lifespan of LHPs. In the two-phase heat transfer devices, NCG is the gas that cannot be condensed to liquid during the operation, and is in the gas state. In general, NCG consists of nitrogen, hydrogen, light hydrocarbons, carbon dioxide or other gaseous materials, depending on the working fluids charged and manufacturing technologies adopted [17, 18]. NCG is mainly produced by the chemical reactions among the impurities introduced into the loop during the machining, cleaning and charging processes, or into the container wall, wick material and the working fluid. Some NCG (mainly air) may also be adsorbed by the wick or container material and diffuse gradually with the circulation of the working fluid over the system's lifetime. Depending on the amount and distribution of NCG in the loop, it can cause difficulty in the startup, increase in the operation temperature and severe performance degradation in the condenser and evaporator. With continuous accumulation of NCG, the thermal performance of LHPs degrades gradually until the failure . As LHPs onboard are generally not allowed to maintain or repair on orbit, the adverse effects of NCG on LHPs are cumulative and irreversible, and it is very important to appropriately

assess the impact of NCG and adopt necessary measures to resolve this issue.

The NCG effect on LHPs has been recently studied both experimentally and theoretically, but the little is known on the NCG effect on the startup of LHPs. For instance Joung et al. [19] noticed that the measured compensation chamber (CC) pressure and the calculated saturation pressure showed similar variation trend with heat load, but having a relatively constant difference around them (7-9 kPa). This was attributed to the existence of NCG. The startup behavior at different elevations showed that the operating temperature overshoot of the LHP exhibited a strong gravity (or elevation) dependence. Singh et al. [20] found that major inventory of NCG was generated during the first a few initial runs of the LHP. The released gas accumulated, in both gaseous and solid metal absorption forms, inside the CC due to the low fluid velocity profile (stagnation conditions) there. It was experimentally deduced that the generation of NCG inside the LHP produced a noticeable increase in the startup time, owing to the requirement of achieving a higher pressure inside the evaporation zone for initiating the fluid circulation in the loop. A failed startup may occur especially under a small heat load condition, which was also confirmed by the experimental results in Ref. [21]. However, in some cases, if some NCG was located in the vapor grooves of the evaporator, the startup might be easier to initiate as it facilitated the evaporation of the working fluid in the evaporator [22, 23]. Aiming to develop a methodology for predicting a "safe start" design envelope for a given system and loop design, Baumann et al.[year] established an analytical model based on the SINDA/FLUINT software, the NASA-standard heat transfer and fluid flow analyzer, to simulate the startup process of LHPs. The effects of NCG, evaporator thermal mass and adverse tilt were taken into account in the model, and preliminary simulation results were reported [24].

As the startup is the first and most important issue to be resolved prior to the engineering application of LHPs in either space or terrestrial surroundings, special attention should be paid to it. However, current studies about the effect of NCG on the startup of LHPs were obviously inadequate. Because the startup of LHPs is a very complex process, in which a variety of heat transfer phenomena such as evaporation, boiling, condensation and convection are involved, accompanied by the liquid/vapor movement and phase redistribution, more detailed and in-depth

studies should be carried out. The objective of this work is to better understand how and to what extent the NCG affects the startup of a LHP, analyze the corresponding physical mechanisms and propose reasonable solutions to solve the NCG issue.

2 Experimental system

2.1 Experimental setup

The tested LHP was made of stainless steel except that the evaporator wick was made of sintered nickel powders, and ammonia was selected as the working fluid due to its excellent thermo-physical properties in the ambient temperature range. Fig. 1(a) shows the schematic of the LHP, and Fig. 2(a) shows the detailed structure of the evaporator and compensation chamber (CC). Table 1 provides the basic parameters of the LHP where OD and ID represent the outer and inner diameters respectively.

Fig. 3 shows the schematic view of the experimental system. Heat load applied to the evaporator was provided by a thin-film electric resistance heater attached to the outer surface of the evaporator, which can be adjusted by altering the output voltage of the DC power in the range of 0-200W. The maximum uncertainty of the heat load was around ±5.0%. The condenser line was brazed with a copper thermal diffusion plate, and the thermal diffusion plate was attached tightly on the two sides of an aluminum cold plate, as shown in Fig. 2(b). The cold plate was cooled by ethanol with a controllable temperature, which was circulating through a refrigerated thermostatic bath. The LHP was placed in a thermal-vacuum chamber where the pressure can be maintained always below 0.01 Pa in the experiments, and all the components were covered with multilayer insulation materials. Twenty three type-T thermocouples with the maximum measurement error of ± 0.5K were employed to monitor the temperature profile along the loop, as illustrated in Fig. 1(b). Temperature data from the thermocouples was recorded, displayed and stored every two seconds by a data acquisition system. To reduce the influence of gravity, the evaporator and the condenser were placed in a horizontal plane in all the experiments.

2.2 Purging and charging process of NCG

In order to clear away as much initial NCG adsorbed at the inner surface of the LHP as possible, a strict purging procedure must be performed before the charging of working fluid into the LHP. Otherwise, the actual amount of NCG in the loop after injection would be larger than the pre-set value. As a common composition of NCG, nitrogen does not react chemically with stainless steel or ammonia and is almost insoluble in liquid ammonia, it was selected as the NCG in this study. The NCG purging and injection system as well as the purging and injection procedures were detailed in our previous paper [25], which is not repeated here. Referring to the results in Ref. [21], the inventory of NCG generated in the LHP at the end of fifteen-year-life was estimated in the order of magnitude of 10^{-5} mol, and a maximum of 8×10^{-5} mol NCG was injected into the LHP with a relative uncertainty of ±3.0%.

3 Experimental results and discussions

The startup of a LHP is a complex dynamic process, ranging from the application of heat load to the evaporator to the normal circulation of working fluid in the loop, which is affected by a variety of factors. It is well accepted that the startup of a LHP is strongly influenced by the liquid/vapor composition in the evaporator, and four possible startup situations have been clearly identified, as shown in Table 2[26-28]. Experiments have shown that LHPs are the easiest to start up in situation 2, but the most difficult in situation 3. Generally, the startup performance of a LHP can be evaluated by three parameters: startup superheat, temperature overshoot and startup time.

A LHP is a passive heat transfer device, and whenever appropriate heat load is applied to the evaporator, it is able to self-start without the need of preconditioning. However, the LHP can be controlled to start up in a specific situation through preconditioning. In the experiment, the preconditioning was conducted as follows: i) a certain heat load to the CC was applied to ensure that the CC temperature was at least 10 K higher than the evaporator temperature for about half an hour; ii) the heating to the CC was terminated and the whole LHP was cooled to the ambient temperature; and iii) specified heat load was applied to the evaporator to start up the LHP. It is of

note that during the heating period to the CC, the working fluid in both vapor grooves and evaporator core was in the subcooled state where the vapor or gas was condensed or collapsed under this condition, the LHP would start up only in situation 1, i.e. both evaporator core and vapor grooves are liquid filled.

3.1 Startup with preconditioning

3.1.1 Effect of NCG inventory

Figs. (4-6) show the temperature variations of a few characteristic points along the loop during the startup of the LHP when 0, 4×10^{-5} and 8×10^{-5} mol NCG were charged into the system, respectively. In Figs. (4-6), the startup heat load was 5W, the heat sink temperature was -15℃, and the other operating conditions were kept all the same except the NCG inventory.

As shown in Fig. 4, when no NCG was charged into the LHP, TC9 on the evaporator rose immediately following the application of the heat load. TC11 at the evaporator outlet remained almost at the ambient temperature, indicating that vapor was not generated in the vapor grooves and pushed into the vapor line. This was because the vapor grooves were completely flooded with liquid, which requires a certain superheat to initiate the nucleate boiling there. At the same time, TCs 3 and 6 on the top and bottom of the CC remained at the ambient temperature, indicating the heat leak from the evaporator to the CC was rather small. This is understandable as the evaporator core was flooded with liquid, and the heat leak from the evaporator to the CC was mainly by the thermal conduction of the evaporator casing and the wick, whose thermal resistance was rather large. From the above temperature variations, it can be inferred that the LHP would start up in situation 1, as expected by preconditioning.

As the evaporator temperature TC9 rose continually, the liquid superheat increased until nucleate boiling occurred in the vapor grooves. The evaporator temperature then dropped sharply due to the absorption of heat by evaporation while the temperature at the evaporator outlet TC11 rose immediately, indicating that vapor generated in the vapor grooves was pushed out of the evaporator and into the vapor line. At the same time, TCs 3 and 6 on the

top and bottom of the CC rose immediately, but TC3 on the top of the CC was obviously higher than TC6 on the bottom of the CC. The reason might be that the superheat was comparatively high when the nucleate boiling occurred, the heat load applied to the evaporator and the sensible heat of the evaporator were both utilized to evaporate the liquid in the vapor grooves, as shown in Equation (1):

$$Q_e = Q_{ap} - (mC_p)_e \times \frac{dT_e}{dt} \quad (1)$$

where Q_e is the heat load for evaporation; Q_{ap} is the heat load applied to the evaporator; $(mC_p)_e$ is the thermal capacity of the evaporator; T_e is the evaporator temperature and t is the time.

At the moment of the onset of nucleate boiling, a large amount of vapor was generated in the vapor grooves, which resulted in a relatively very high pressure at the outer surface of the wick. Under such a high pressure condition, some of the vapor would penetrate the porous wick and go through the evaporator core to the vapor region of the CC, leading to a sharp increase of heat leak from the evaporator to the CC. This was confirmed by the fact that the maximum temperature rise of TC3 on the top of the CC was almost the same as that of TC11 at the evaporator outlet, while the maximum temperature rise of TC6 on the bottom of the CC was obviously smaller because it represented the liquid temperature in the CC in ground tests. Other part of the vapor would flow out of the evaporator and into the vapor line, then enter the condenser line, resulting in a rapid and large temperature rise at the condenser inlet (TC12) followed by the quick temperature drop at the CC inlet (TC1). With the circulation of the working fluid in the loop, the temperatures of the evaporator and CC began to drop very slowly until the LHP achieved the steady state operation. It was believed that this was caused by a slightly larger return subcooling compared with the heat leak from the evaporator to the CC.

As shown in Figs. 5 and 6, when 4×10^{-5} and 8×10^{-5} mol NCG were charged into the LHP, the temperature variation trends along the loop were very similar to those in Fig. 4, indicating that the LHP started up in situation 1. However, the startup performance of the LHP in Figs. 5 and 6 became much worse than that in Fig. 4, as summarized in Table 3. Especially when 8×10^{-5} mol NCG was charged into the LHP, the temperature overshoot was increased from 7.1 to 21.8℃, the liquid superheat was increased from 6.7 to 19.7℃, and the startup time was

increased from 84 to 270 seconds, as compared with the case of non NCG, Figure 4. From Table 3, it can be concluded that the NCG exhibits a significant adverse effect on the startup performance, and the more the NCG exists in the LHP, the higher the temperature overshoot and liquid superheat, and the longer the startup time required.

The adverse influence of NCG is believed to be related to the increased pressure effect in the CC. Under the effect of preconditioning, the working fluid in the whole loop excluding the CC would be in the subcooled state, i.e., the vapor or gas was condensed or collapsed. The majority of the NCG should be located in the vapor region of the CC, which led to much elevated pressure in the CC due to the partial pressure generated by the NCG:

$$P_{CC} = P_{v,sat} + P \quad (2)$$

Prior to the circulation of working fluid in the loop, the pressure in each component should be all the same, so the liquid in the evaporator was in the subooled state with a subcooling of :

$$\Delta T_{sub} = \left(\frac{dT}{dP}\right)_{sat} \times P_{NCG} \quad (3)$$

This would result in a direct increase of the temperature overshoot during the startup as the evaporator temperature had to increase first to the corresponding saturation temperature, and then attain the required superheat to initiate the nucleate boiling in the vapor grooves. The higher the partial pressure of NCG in the CC, the larger the subcooled degree of the liquid in the evaporator, and the larger the temperature overshoot. At the same time, the existence of NCG in the CC would lead to much increased liquid superheat and delayed onset of nucleate boiling in the vapor grooves, resulting in an increased startup time accordingly.

3.1.2 Effect of startup heat load

Figs. 7 and 8 show the temperature variations of some characteristic points along the loop during the startup of the LHP when 4×10^{-5} mol NCG was charged into the system, the heat sink temperature was -15℃, and the startup heat loads were 10 and 20 W respectively. Comparing Figs. 7 and 8 with Fig. 5, the temperature variation trends of

the characteristic points were quite similar, but the startup performance was quite different. The larger the startup heat load, the better the startup performance, as summarized in Table 3. When the startup heat load was increased from 5 W to 20 W, the temperature overshoot was decreased from 16.3 to 9.5 ℃, the liquid superheat was decreased from 13.8 to 9.3℃, and the startup time was reduced from 190 to 40 seconds. It can be concluded that a larger startup heat load contributes to better startup performance in the presence of NCG. . Proper management of the heat load could be a possible solution to mitigate the adverse effect of NCG on the startup performance.

3.1.3 Effect of heat sink temperature

Fig. 9 shows the temperature variations of some characteristic points along the loop during the startup of the LHP when 4×10^{-5} mol NCG was charged into the system, the startup heat load was 5 W, and the heat sink temperature was 15℃. The comparison of Fig. 9 and Fig. 5 shows that the influence of heat sink temperature is small. Both the temperature variation trends during the and the startup performance were similar regardless of the heat sink temperature. The differences in the temperature overshoot, liquid superheat and startup time were within 0.6 ℃, 0.8 ℃ and 2 seconds, respectively. Such a result suggests that the heat sink temperature exhibits very slight influence on the startup performance in the presence of NCG, which can be generally neglected. The result is expected as the heat sink almost imposed no influence on the heat and mass transfer of the evaporator and CC before the working fluid circulation. The effect only became salient after the startup, i.e. reaching a steady circulation of the working fluid in the loop.

3.2 Startup without preconditioning

When a LHP starts up without preconditioning, four possible situations may exist theoretically, as listed in Table 2. However, through the match design of the working fluid inventory and CC volume, it can be guaranteed that the liquid/vapor interface level in the CC is always higher than the top of the evaporator core even the external loop is completely flooded with liquid. Under such a condition, the evaporator core is always filled with liquid, and the

startup can only occur in situation 1 or 2, thus the most difficult startup, i.e. in situation 3, can be effectively avoided. Experimental results confirmed the above analysis. When no NCG was charged into the system, the LHP started up in situation 1 in most of the cases. Only in rare cases that the LHP started up in situation 2, and no startups in situation 3 or 4 was observed, similar to our previous results [ref]. However, when NCG was charged into the system, the situation became quite different, and the LHP was observed to start up possibly in situations 1, 3 or 4, as described below.

3.2.1 Startup in situation 1

Figs. 10 and 11 show the temperature variations during the startup of the LHP without preconditioning when no NCG and 4×10^{-5} mol NCG was charged into the system, respectively. Here the startup heat load was 20 W, and the heat sink temperatures were 5 and -15℃ respectively. The results were very similar to those in Figs (4-6) with preconditioning, indicating that the startup was in situation 1. However the existence of NCG resulted in considerable performance degradation of the startup as analyzed in section 3.1.1 above.

3.2.2 Startup in situation 3

Fig. 12 shows the temperature variations of characteristic points at a NCG concentration of 6×10^{-5} mol, startup heat load of 20 W and heat sink temperature of -15℃. It shows that when heat load was applied to the evaporator, TC9 on the evaporator rose immediately while TC11 at the evaporator outlet remained almost at the ambient temperature, indicating that no vapor was presenting in the vapor grooves. However the temperature on the top of the CC (i.e. TC3) also rose immediately following the increase of TC9 , while TC6 on the bottom of the CC was obviously lower than TC3. This suggests that the heat leak from the evaporator to the CC was very large, due to the existence of vapor or gas exists in the evaporator core. The heat leak from the evaporator to the CC was in the form of liquid evaporation in the evaporator core and subsequent vapor condensation in the upper space of the CC, in a process similar to a traditional heat pipe. It appears that the LHP has started up in in situation 3, i.e.,

the most difficult startup case.

As the evaporator temperature continued to rise to about 48 ^{o}C, the temperature at the evaporator outlet (i.e. TC11) increased sharply, followed by TC12 at the condenser inlet, which indicates the onset of nucleate boiling in the vapor grooves. The generated vapor was pushed out of the evaporator and entered the condenser through the vapor line, establishing a normal fluid circulation in the loop. At the same time, the temperatures of the evaporator and CC began to drop gradually due to the absorption of heat by evaporation and the cooling to the CC by the return subcooling respectively, until the LHP achieved a steady state operation. Although the LHP finally started up successfully in situation 3, the temperature overshoot was very large, i.e. > 25 ^{o}C, and the maximum evaporator temperature was beyond 50 ^{o}C.

In addition, Fig. 12 demonstrated that nucleate boiling could occur in the vapor grooves even the evaporator temperature rose at the same rate as that of the CC, i.e. the temperature difference between them or the liquid superheat remained constant. As there was no pressure measurement in the evaporator, it is hard to explain definitely. One possible reason may be that the liquid superheat required to initiate the nucleate boiling became reduced as its temperature rises. The superheat of liquid to initiate nucleate boiling can be expressed by Equation (4):

$$\Delta T_{sup} = \left(\frac{dT}{dP}\right)_{sat} \times \Delta P = \frac{T_{sat} v_{fg}}{h_{fg}} \times \frac{2\sigma}{r_n} \tag{4}$$

where T_{sat} is the saturation temperature of vapor; v_{fg} is the difference of the specific volume between saturated vapor and liquid; h_{fg} is the latent heat of vaporization; σ is the surface tension and r_n is the nucleate radius. These thermophysical properties are strong functions of temperature. As the liquid temperature rises, T_{sat} increases but v_{fg}, h_{fg} and σ decrease, with an possible effect of reducing ΔT_{sup}.

From section 3.1.2 above, it shows that a larger startup heat load contributes to a better startup performance in situation 1, and the effect of startup heat load in situation 3 was also examined , as shown in Fig. 13. With the increase of heat load from 20W to 80W, , the startup time was reduced significantly, i.e., from 130s to 80s, but the

temperature overshoot was only decreased by ~ 3℃. This suggests that the improvement of the startup performance in situation 3 by increasing the heat load was not as effective as that in situation 1. Under this condition, a thermoelectric cooler may be employed to actively cool the CC to inhibit the adverse effect of NCG and enhance the startup performance.

3.2.3 Startup in situation 4

Fig. 14 shows the temperature variations of some characteristic points during the startup of the LHP where the operating conditions were all the same as those in Fig. 12. When heat load was applied to the evaporator, TC9 on the evaporator rose immediately followed closely by TC11 at the evaporator outlet, indicating that vapor was generated immediately in the vapor grooves and was pushed into the vapor line. This suggests that vapor or gas existed in the vapor grooves, and evaporation occurred once the heat load was applied without requiring additional liquid superheat. Similar to the analysis above, the temperature profiles of TC3, TC6 and TC9 indicated that the heat leak from the evaporator to the CC was relatively large, and there was vapor or gas existing in the evaporator core. Consequently the LHP was started up in situation 4.

With the circulation of the working fluid in the loop, the temperature at the condenser inlet TC12 rose quickly, while the temperature at the CC inlet dropped gradually, indicating that vapor entered the condenser and the condensate flowed towards the CC through the liquid line. The temperatures of the evaporator and CC began to drop very slowly until the LHP achieved the steady state operation, which was caused by a slightly larger return subcooling compared with the heat leak from the evaporator to the CC. From Fig. 14, it can be concluded that although NCG exists in the LHP, a very favorable startup can be expected if the startup proceeds in situation 4, even better than the case without NCG.

4 Conclusions

In this work, an extensive experimental study was conducted to reveal how and to what extent NCG may affect

the startup performance of a LHP with and without preconditioning. The temperature overshoot, liquid superheat and startup time were employed as the evaluation criteria, and the main conclusions are summarized as follows:

- With NCG presence in the LHP, the startup can only proceed in situation 1 with preconditioning; while it may proceed in situations 1, 3 or 4 without preconditioning.
- For the startup in situation 1, a larger NCG inventory led to much degraded startup performance, and a higher startup heat load was beneficial to the startup, but the effect of heat sink temperature on the startup was small. .
- For the startup in situation 3, i.e., the most difficult startup situation, NCG produced a very high temperature overshoot during the startup, which may even exceed the maximum allowable temperature and cause the startup failure.
- For the startup in situation 4, the existence of NCG in the vapor grooves could facilitate the evaporation of liquid, generating a desirable startup, which generally does not occur when no NCG was present. .

Acknowledgements

This work was supported by the National Natural Science Foundation of China (No. 51306009 and 51406009) and the EU Marie Curie Actions-International Incoming Fellowships (FP7-PEOPLE-2013-IIF-626576). The authors are very grateful to Lei Li, Lizheng Zong, Guoguang Li and Taihui Du in the Beijing Institute of Spacecraft System Engineering, China Academy of Space Technology, for their help in the preparation of the experiments.

Nomenclature

C_p	specific heat (J/kg·K)
h	enthalpy ((J/kg)
m	mass (kg)
P	pressure (Pa)
Q	heat load (W)
r	radius (m)
T	temperature (K)
t	time (s)
v	specific volume (m^3/kg)
σ	surface tension (N/m)

Subscripts

ap	Applied
CC	compensation chamber
Cond	condenser
EV	Evaporator
e	evaporation or evaporator
fg	difference between vapor and liquid
n	Nucleate
NCG	non-condensable gas
sat	Saturation
sub	Subcooled
sup	Superheat
VL	vapor line
v	Vapor

References

[1] Y. F. Maydanik, Loop heat pipes, Applied Thermal Engineering 25(2005) 635-657.

[2] Jentung Ku, Operating Characteristics of Loop Heat Pipes. SAE Paper, No.1999-01-2007, 1999.

[3] G.H. Wang, D. Mishkinis, D. Nikanpour, Capillary heat loop technology: space applications and recent Canadian activities, Applied Thermal Engineering 28(2008) 284-303.

[4] L. Bai, G. Lin, D. Wen, et al., Experimental investigation of startup behaviors of a dual compensation chamber loop heat pipe with insufficient fluid inventory, Applied Thermal Engineering 29(2009)1447–1456.

[5] N. Wang, Z. Cui, J. Burger, et al., Transient behaviors of loop heat pipes for alpha magnetic spectrometer cryocoolers, Applied Thermal Engineering 68 (2014) 1-9.

[6] Y.F. Maydanik, M.A. Chernysheva, V.G. Pastukhov, Review: Loop heat pipes with flat evaporators, Applied Thermal Engineering 67 (2014) 294-307.

[7] Eric W. Grob, Mission Performance of the GLAS Thermal Control System - 7 Years In Orbit. AIAA Paper, No.2010-6029.

[8] Charles Baker, Dan Butler, Eric Grob, et al., Geoscience Laser Altimetry System (GLAS) Loop Heat Pipe Anomaly and On Orbit Testing, AIAA 2011-5209, 41st International Conference on Environmental Systems 17 - 21 July 2011, Portland, Oregon.

[9] Michael K. Choi, Swift BAT Loop Heat Pipe #0 Temperature Drop Problem and Solution after Its Primary Heater Controller Failure, AIAA 2011-5098, 41st International Conference on Environmental Systems 17 - 21 July 2011, Portland, Oregon.

[10] Triem T. Hoang, William J. Armiger, Robert W. Baldauff, et al., Performance of COMMx Loop Heat Pipe on TacSat 4 Spacecraft. AIAA Paper, No. 2012-3498.

[11] J. Feng, G. Lin, L. Bai, Experimental investigation on operating instability of a dual compensation chamber loop heat pipe, Science in China Series E: Technological Sciences 52(2009) 2316-2322

[12] G. Lin, N. Li, L. Bai, et al., Experimental investigation of a dual compensation chamber loop heat pipe, International Journal of Heat and Mass Transfer 53(2010) 3231-3240

[13] P.D. Dunn, D.A. Reay, Heat Pipes, Pergamon, London, 1994.

[14] A. Faghri, Heat Pipe Science and Technology, Taylor & Francis, London, 1995.

[15] S.P. Sorensen, J. Smith, J.P. Zarling, Thermal performance of TAPS heat pipes with non condensable gas blockage, cold regions impacts on transportation and infrastructure, in: Proceedings of 11th International Conference, ASCE, Anchorage AK, May 2002, pp. 1-12.

[16] C.J. Tu, C.Y. Wang, Noncondensable gas effect on condensation in a separate type two-phase closed thermosyphon, Heat Mass Transfer 23 (3) (1988) 153-158.

[17] J. He, G. Lin, L. Bai, et al., Effect of non-condensable gas on startup of a loop thermosyphon, International Journal of Thermal Sciences 72 (2013) 184-194.

[18] J. He, G. Lin, L. Bai, et al., Effect of non-condensable gas on steady-state operation of a loop thermosyphon, International Journal of Thermal Sciences 81 (2014) 59-67.

[19] Wukchul Joung, Taeu Yu, Jinho Lee, Experimental study on the operating characteristics of a flat bifacial evaporator loop heat pipe, International Journal of Heat and Mass Transfer 53(2010) 276–285.

[20] Randeep Singh, Aliakbar Akbarzadeh, Masataka Mochizuki, Operational characteristics of the miniature loop heat pipe with non-condensable gases, International Journal of Heat and Mass Transfer 53(2010) 3471–3482.

[21] M. N. Nikitkin, W. B. Bienert, K. A. Goncharov, Non-condensable gases and loop heat pipe operation, SAE Paper, No. 981584,1998.

[22] Kimberly R. Wrenn, David A. Wolf, Edward J. Kroliczek, Effect of noncondensible gas and evaporator mass on loop heat pipe performance. SAE Paper, No. 2000-01-2409, 2000.

[23] D. Mishkinis, G. Wang, D. Nikanpour, et al., Advances in two-phase loop with capillary pump technology and space applications. SAE Paper, No. 2005-01-2883.

[24] J. Baumann, B. Cullimore, B. Yendler, et al., Noncondensible gas, mass, and adverse tilt effects on the start-up of loop heat pipes. SAE Paper, No. 1999-01-2048.

[25] J. He, G. Lin, L. Bai, et al., Effect of non-condensable gas on the operation of a loop heat pipe, International Journal of Heat and Mass Transfer 70(2014) 449-462.

[26] M.L. Parker, Modeling of loop heat pipe with applications to spacecraft thermal control, Pennsylvania: Faculty of Mechanical

Engineering and applied Mechanics, University of Pennsylvania, 2000

[27] T.T. Hoang, R.W. Baldauff, K.H. Cheung, Start-up behavior of an ammonia loop heat pipe, AIAA paper, No. 2005-5630

[28] H.X. Zhang, G.P. Lin, T. Ding, et al., Investigation of startup behaviors of a loop heat pipe, Journal of Thermophysics and Heat Transfer 19 (4) (2005) 509-518.

Table captions

Figure captions:

Fig. 1 Schematic of the tested LHP and thermocouple locations

Fig. 2 Detailed structures of the evaporator, CC and condenser

Fig. 3 Schematic of the experimental system

Fig. 4 Startup with preconditioning (Q_{ap}=5W, T_s=-15℃, without NCG)

Fig. 5 Startup with preconditioning (Q_{ap}=5W, T_s=-15℃, NCG=4×10^{-5}mol)

Fig. 6 Startup with preconditioning (Q_{ap}=5W, T_s=-15℃, NCG=8×10^{-5}mol)

Fig. 7 Startup with preconditioning (Q_{ap}=10W, T_s=-15℃, NCG=4×10^{-5}mol)

Fig. 8 Startup with preconditioning (Q_{ap}=20W, T_s=-15℃, NCG=4×10^{-5}mol)

Fig. 9 Startup with preconditioning (Q_{ap}=5W, T_s=15℃, NCG=4×10^{-5}mol)

Fig. 10 Startup in situation 1 without preconditioning (Q_{ap}=20W, T_s=5℃, no NCG)

Fig. 11 Startup in situation 1 without preconditioning (Q_{ap}=20W, T_s=-15℃, NCG=4×10^{-5}mol)

Fig. 12 Startup in situation 3 without preconditioning (Q_{ap}=20W, T_s=-15℃, NCG=6×10^{-5}mol)

Fig. 13 Startup in situation 3 without preconditioning (T_s=-15℃, NCG=6×10^{-5}mol)

Fig. 14 Startup in situation 4 without preconditioning (Q_{ap}=20W, T_s=-15℃, NCG=6×10^{-5}mol)

Table1 Basic parameters of the tested LHP

Components	Parameters
OD/ID×Length of evaporator/mm	13/11×130
OD/ID×Length of wick/mm	11/4×100
OD/ID×Length of vapor line/mm	3/2×800
OD/ID×Length of condenser/mm	3/2×1010
OD/ID×Length of liquid line/mm	3/2×500
Volume of CC/ml	15.26
Working fluid inventory/g	15.0
Porosity of wick	55%
Number×height×width of Grooves/mm	8×1×1

Table 2 Liquid/vapor composition in the evaporator

Situations	Vapor grooves/evaporator core
1	Liquid filled/liquid filled
2	Vapor exists/ liquid filled
3	Liquid filled /vapor exists
4	Vapor exists/vapor exists

Table 3 Startup performance with preconditioning

NCG inventory /10^{-5}mol	Heat load /W	Heat sink temperature /℃	Temperature overshoot /℃	Liquid superheat /℃	Time /s
0	5	-15	7.1	6.7	84
4	5	-15	16.3	13.8	190
8	5	-15	21.8	19.7	270
4	10	-15	12.5	12.3	72
4	20	-15	9.5	9.3	40
4	5	15	15.7	14.6	188

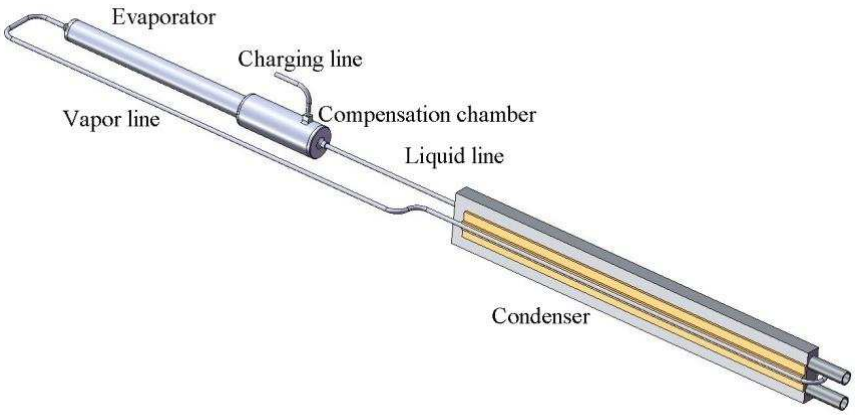

(a) Schematic of the tested loop heat pipe

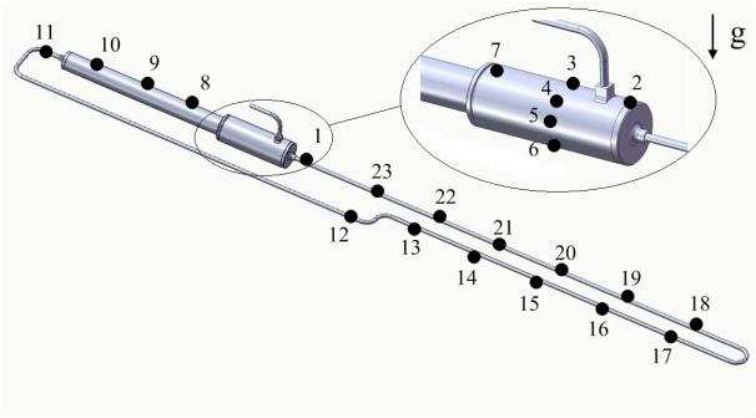

(b) Thermocouple locations along the loop

Fig. 1 Schematic of the tested LHP and thermocouple locations

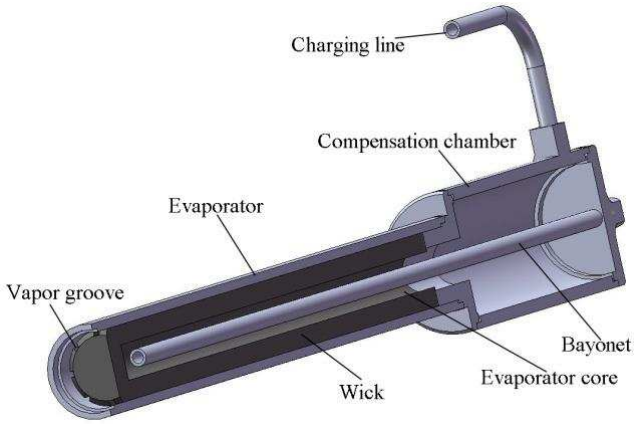

(a) Cross section of the evaporator and CC

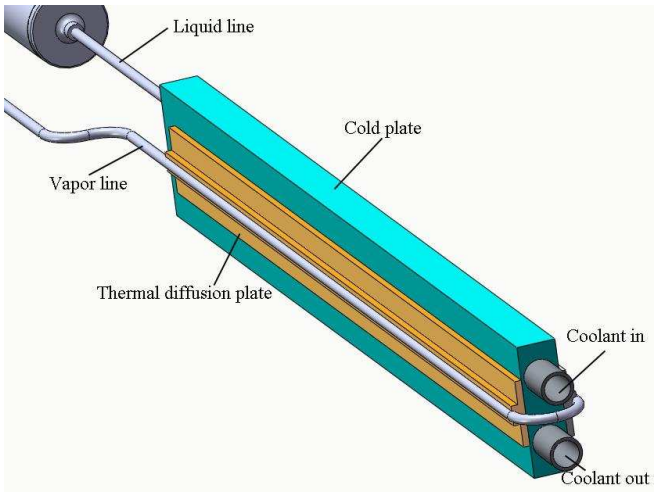

(b) Schematic of the condenser and cold plate

Fig. 2 Detailed structures of the evaporator, CC and condenser

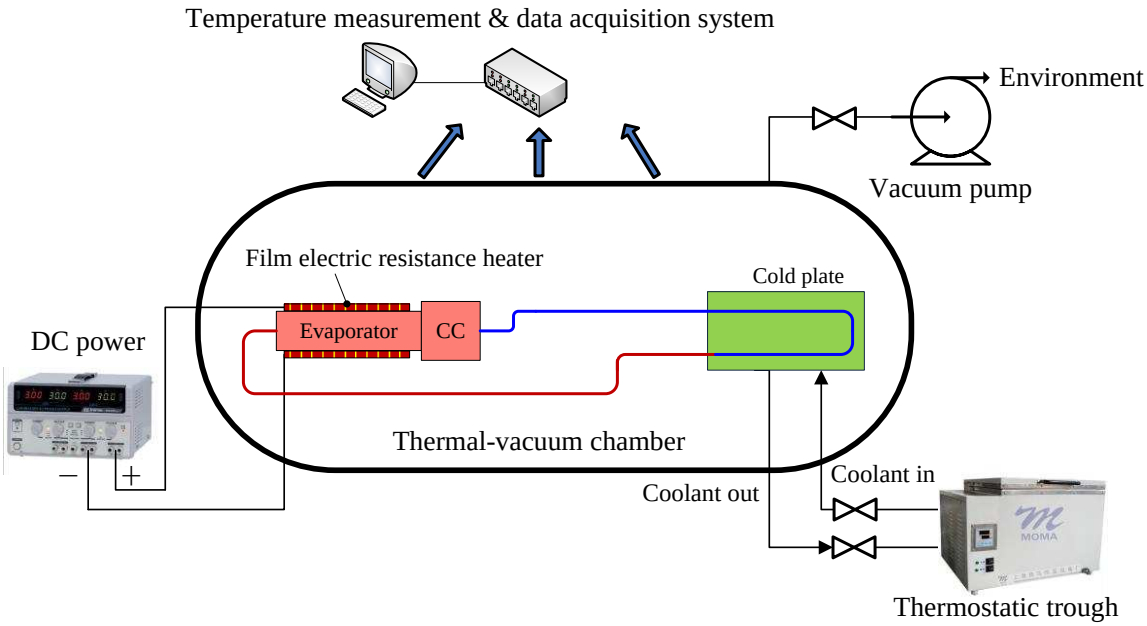

Fig. 3 Schematic of the experimental system

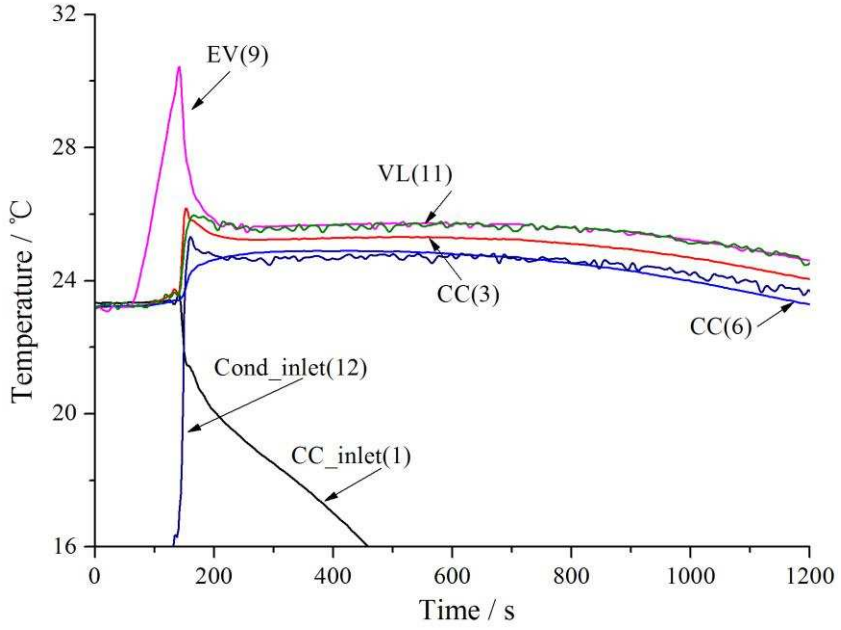

(a) whole range

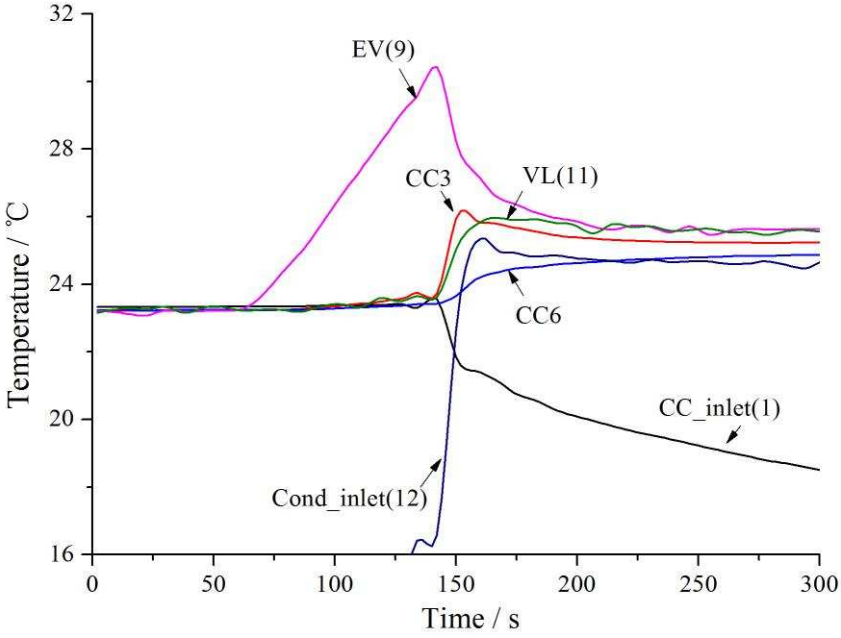

(b) local enlargement

Fig. 4 Startup with preconditioning (Qap=5W, Ts=-15℃, without NCG)

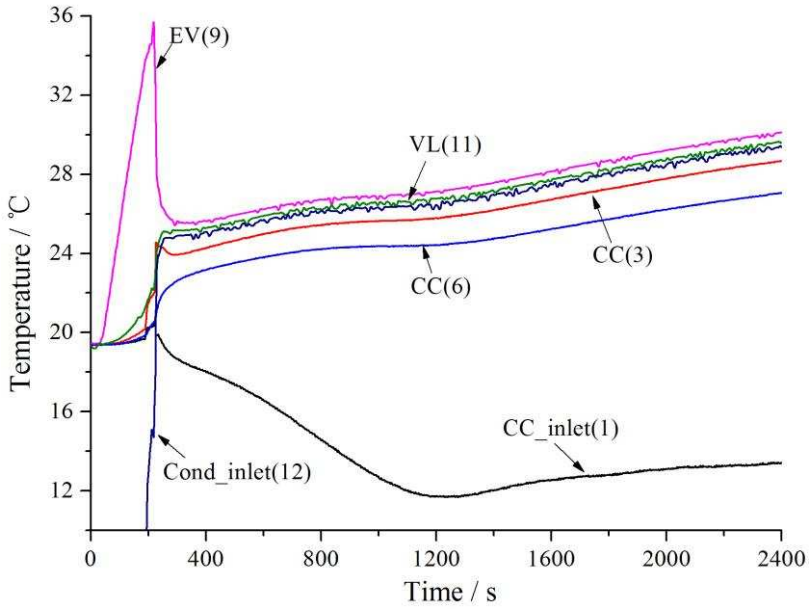

(a) whole range

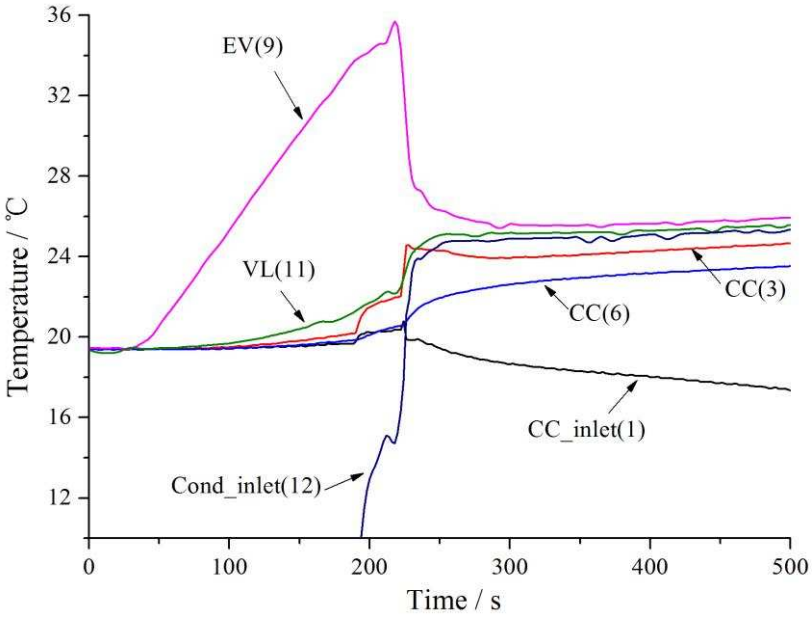

(b) local enlargement

Fig. 5 Startup with preconditioning (Q_{ap}=5W, T_s=-15℃, NCG=4×10^{-5}mol)

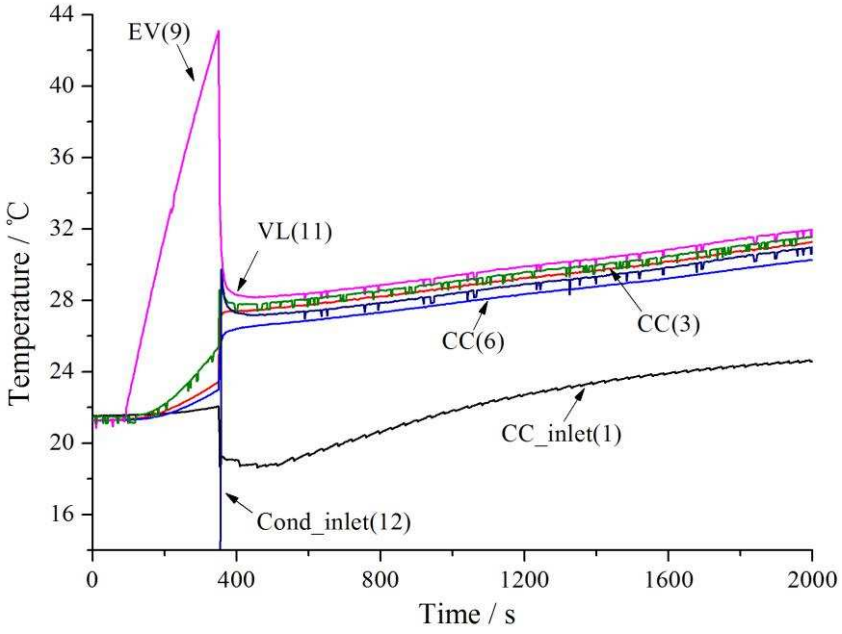

(a) whole range

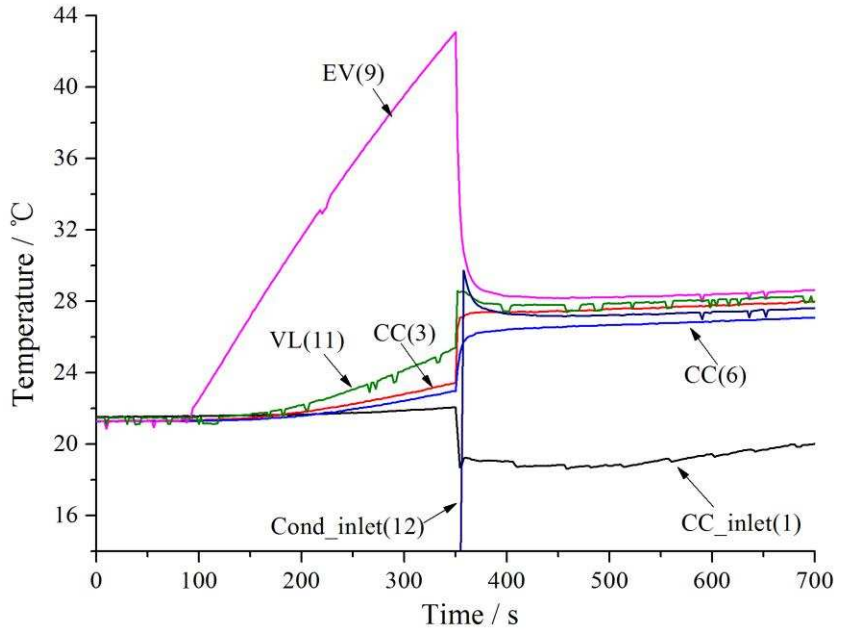

(b) local enlargement

Fig. 6 Startup with preconditioning (Qap=5W, Ts=-15℃, NCG=8×10^{-5}mol)

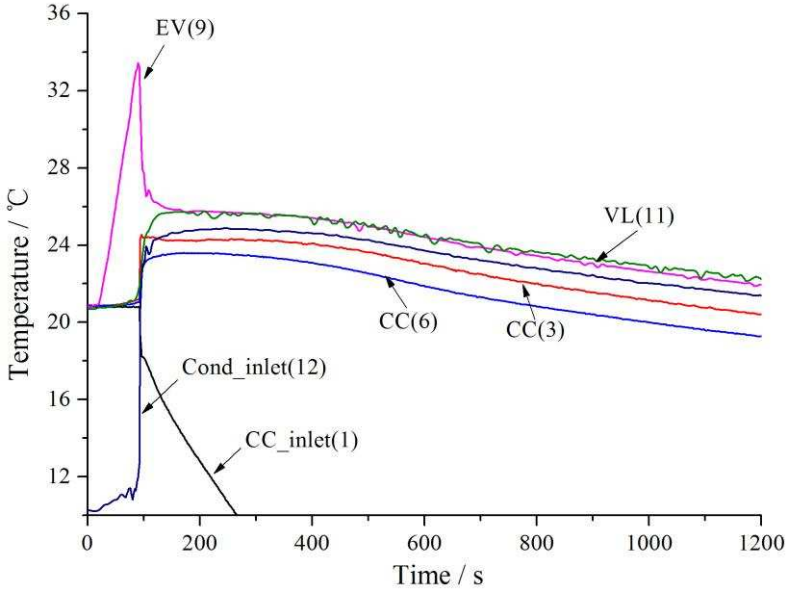

Fig. 7 Startup with preconditioning (Qap=10W, Ts=-15℃, NCG=4×10^{-5}mol)

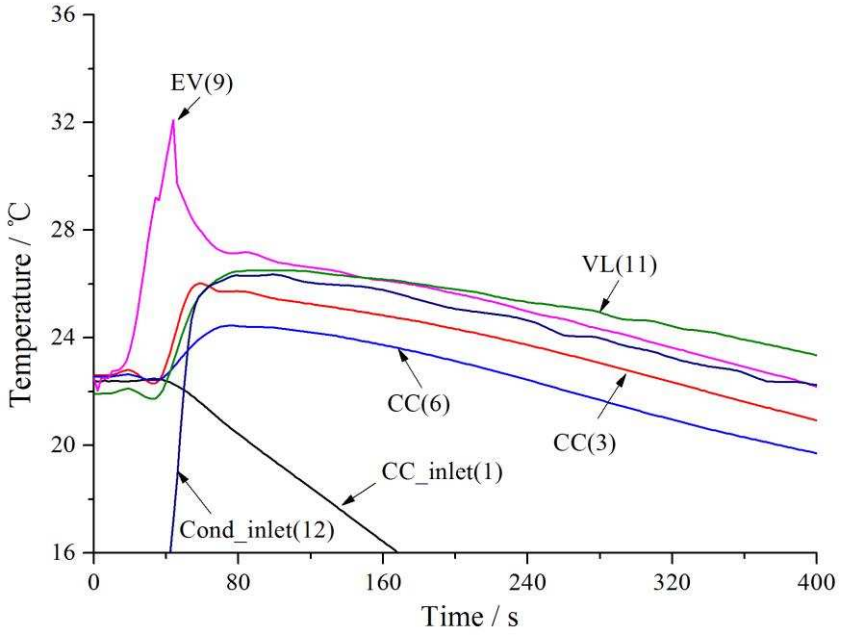

Fig. 8 Startup with preconditioning (Qap=20W, Ts=-15℃, NCG=4×10^{-5}mol)

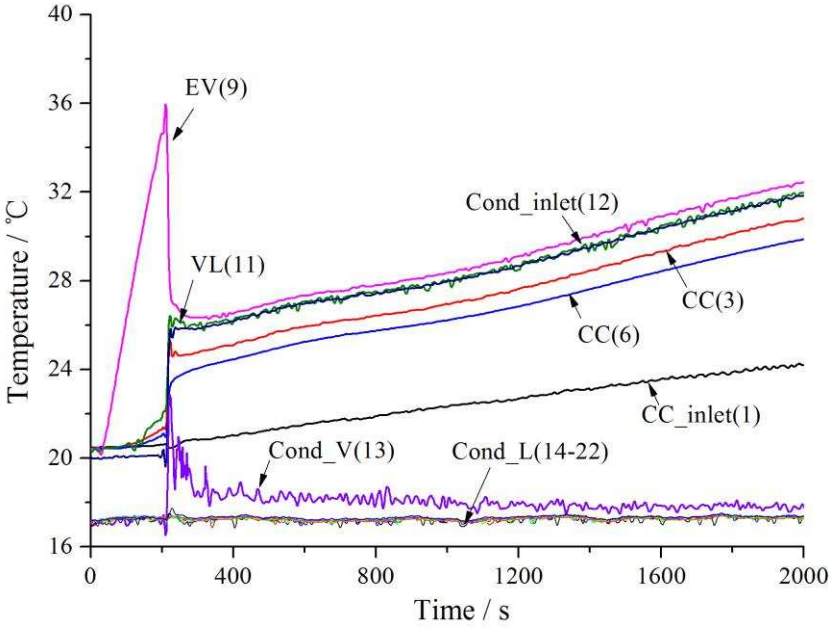

Fig. 9 Startup with preconditioning (Qap=5W, Ts=15℃, NCG=4×10^{-5}mol)

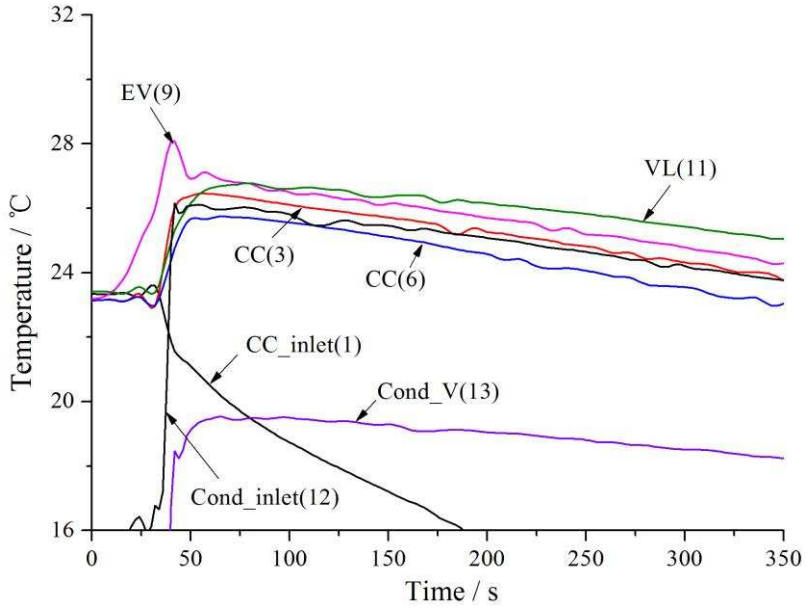

Fig. 10 Startup in situation 1 without preconditioning (Qap=20W, Ts=5℃, no NCG)

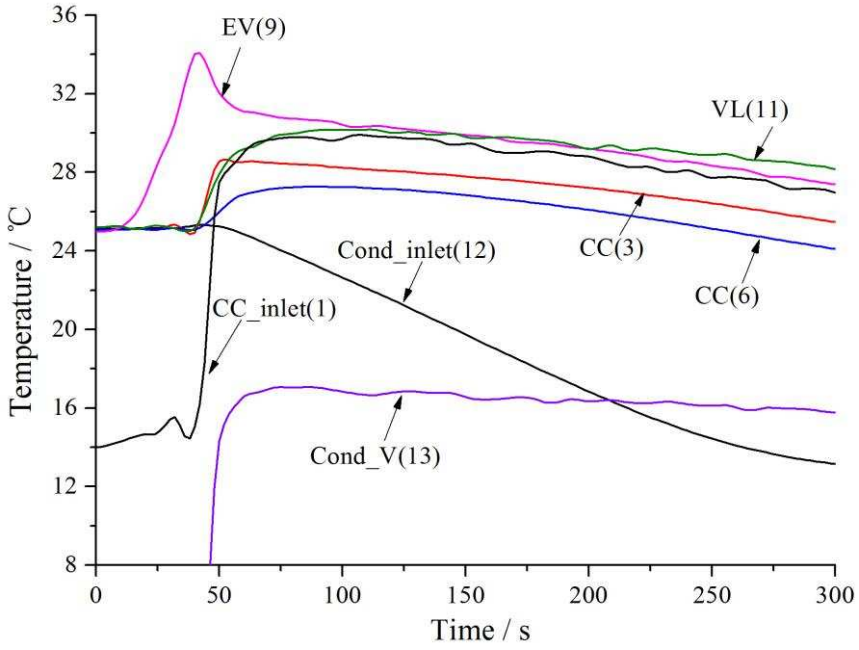

Fig. 11 Startup in situation 1 without preconditioning (Qap=20W, Ts=-15℃, NCG=4×10^{-5}mol)

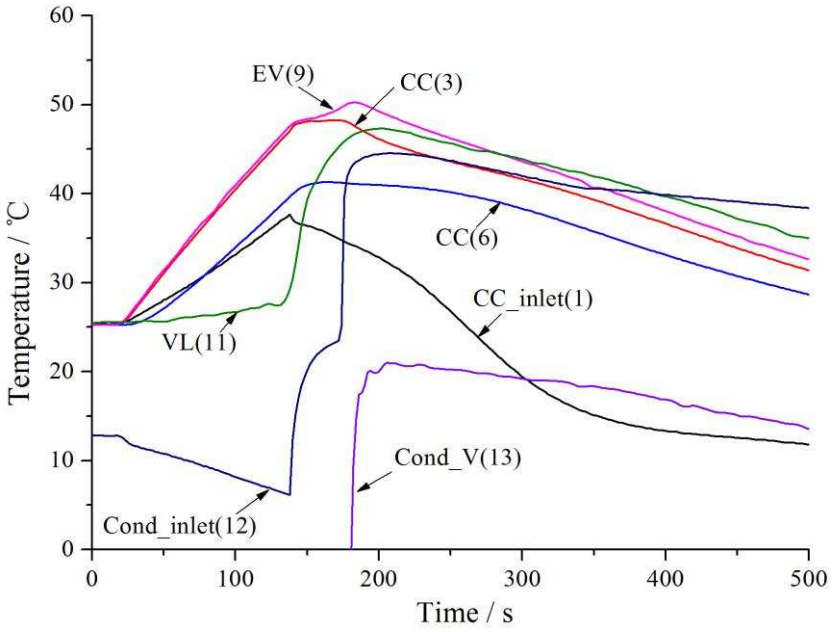

Fig. 12 Startup in situation 3 without preconditioning (Qap=20W, Ts=-15℃, NCG=6×10^{-5}mol)

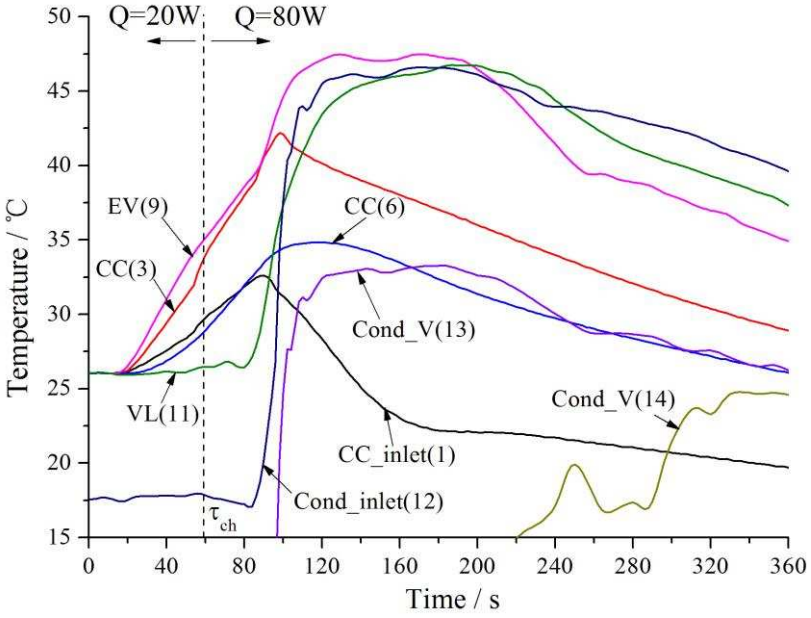

Fig. 13 Startup in situation 3 without preconditioning (Ts=-15℃, NCG=6×10^{-5}mol)

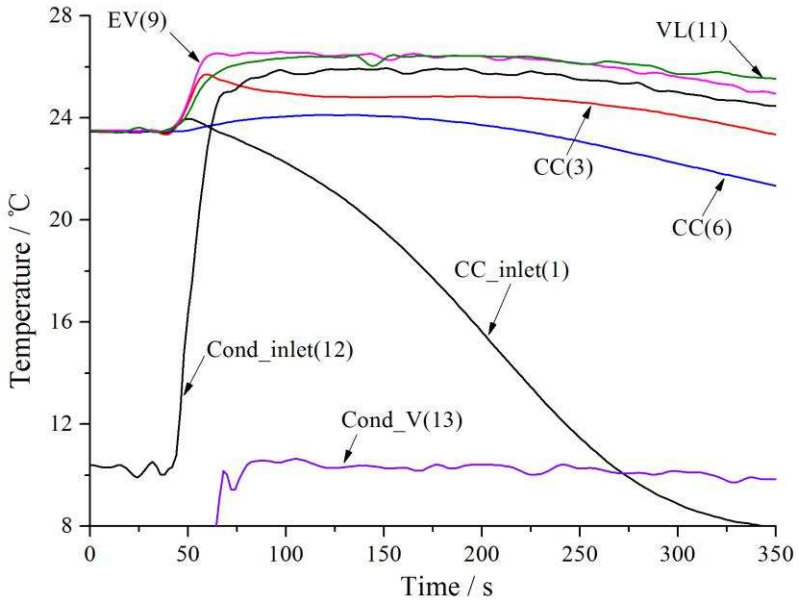

(a) whole range

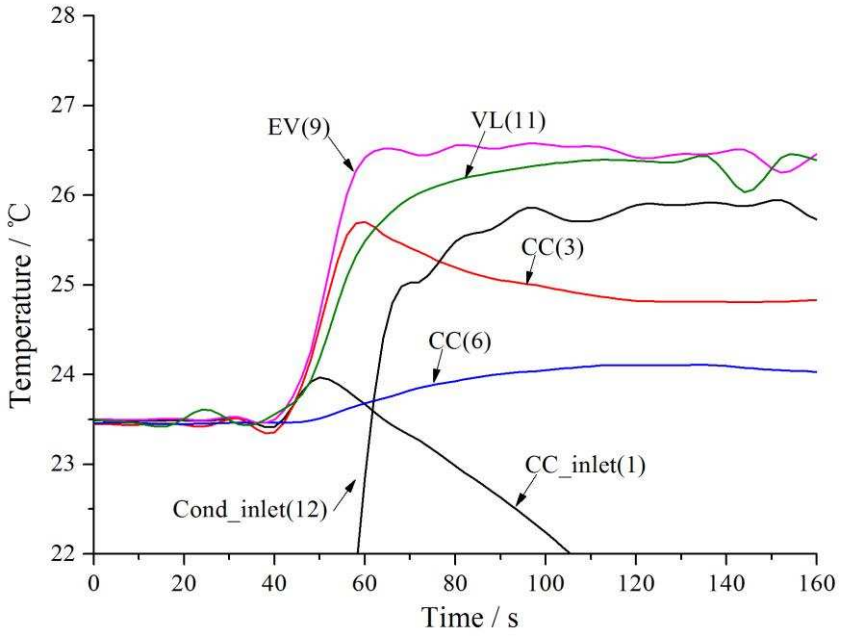

(b) local enlargement

Fig. 14 Startup in situation 4 without preconditioning (Qap=20W, Ts=-15℃, NCG=6×10^{-5}mol)